



## City Research Online

### City, University of London Institutional Repository

---

**Citation:** Manolesos, M. & Voutsinas, S. G. (2016). Experimental study of drag-reduction devices on a flatback airfoil. *AIAA Journal*, 54(11), pp. 3382-3396. doi: 10.2514/1.j054901

This is the accepted version of the paper.

This version of the publication may differ from the final published version.

---

**Permanent repository link:** <https://openaccess.city.ac.uk/id/eprint/27011/>

**Link to published version:** <https://doi.org/10.2514/1.j054901>

**Copyright:** City Research Online aims to make research outputs of City, University of London available to a wider audience. Copyright and Moral Rights remain with the author(s) and/or copyright holders. URLs from City Research Online may be freely distributed and linked to.

**Reuse:** Copies of full items can be used for personal research or study, educational, or not-for-profit purposes without prior permission or charge. Provided that the authors, title and full bibliographic details are credited, a hyperlink and/or URL is given for the original metadata page and the content is not changed in any way.

# Experimental Study of Drag Reduction Devices on a Flatback Airfoil

Marinos Manolesos<sup>1,2</sup> and Spyros G. Voutsinas<sup>3</sup>

*National Technical University of Athens, Greece*

Various trailing edge drag reduction devices, including a new Flap device, were examined experimentally on a flatback airfoil in a wind tunnel. The tests concerned a 30% thick airfoil with 10.6% thick trailing edge. Pressure, Hot Wire and Stereo PIV measurements were performed at a chord Reynolds number of  $Re_c = 1.5e6$ . Results show that the best performing devices decrease drag, increase the vortex shedding frequency and reduce flow variation downstream of the wing trailing edge. The best performing device was a combination of the Flap with an Offset Cavity plate. Further investigation is required for the optimization of the new device and in order to examine its effects on noise reduction, load mitigation and control.

## I. Nomenclature

$A$	=	frequency amplitude
$A_{max}$	=	maximum frequency amplitude for the plane airfoil
$C_d$	=	drag coefficient
$C_l$	=	lift coefficient
$C_{lmax}$	=	maximum lift coefficient

---

<sup>1</sup> Researcher, Laboratory of Aerodynamics, Mechanical Engineering Department, Iron Polytechniou 9, 15780, Athens, Greece, AIAA Member.

<sup>2</sup> Aerodynamics Expert, FLOWFIELD Private Company, Athens, Greece

<sup>3</sup> Professor, Laboratory of Aerodynamics, Mechanical Engineering Department, Iron Polytechniou 9, 15780, Athens, Greece, AIAA Member.

$C_p$	=	pressure coefficient
$c$	=	airfoil chord
$f$	=	frequency
$h$	=	trailing-edge (TE) height
$L/D$	=	lift to drag ratio
$Re_c$	=	Reynolds number based on chord length and free stream velocity
$St$	=	Strouhal number
$U_\infty$	=	free stream velocity
$U$	=	streamwise velocity component
$U_{res}$	=	minimum resolved velocity
$X$	=	streamwise coordinate
$\alpha$	=	angle of attack
$\alpha_{Clmax}$	=	angle of attack at which the maximum lift coefficient value is observed
$\varphi$	=	angle between the two Stereo PIV cameras

## II. Introduction

As wind turbines increase in size, designing blades with minimal weight and adequate stiffness becomes a challenge. In this respect, the use of flatback (FB) airfoils has been proposed as a solution as FB profiles have large cross sectional area and better structural characteristics compared to their sharp Trailing Edge (TE) counterparts. At the same time flatback profiles are less demanding in terms of pressure recovery and hence have reduced leading-edge (LE) roughness sensitivity [1]. In addition they have increased maximum lift compared to thin TE airfoils of the same thickness [2, 3]. This, however, comes with a significant drag penalty, mainly due to base drag, which can be reduced by means of various TE add-ons [4].

The objective of the present study is dual. First it aims at examining whether a new flap device can provide improved performance for a non-symmetric flatback airfoil. The performance of the new device is compared to that of other drag reduction configurations that have shown promising results in the past, such as the TE splitter and the TE cavities. The second objective is to examine the physics that underlie the drag reduction mechanism for different devices. To achieve both ends, pressure, hot wire anemometry and Stereo Particle Image Velocimetry (PIV) measurements have been performed.

In the following section a brief review of relevant studies is given followed by a description of the experimental set-up in Section IV. Results are presented and discussed in Section V and the paper closes with the conclusions given in Section VI.

### III. Background

In the wake of bluff bodies a vortex street is formed, which is linked to the low pressure region close to the body TE and which leads to high drag values [5]. Ways to reduce this significant drag force in sub-sonic flow have been investigated for more than four decades [5-7]. The most common passive drag reduction technique is to alter the bluff body wake by means of various devices located at the body TE or different TE modifications. The modifications aim at increasing base pressure and thus reducing base drag. The increase in base pressure is achieved either by the displacement of the low pressure vortex street downstream, away from the base surface [8] or by the creation of streamwise vorticity [9].

Bearman [10] found that the base pressure is inversely proportional to the formation length, which is defined as the distance from the TE to the point where the velocity fluctuation level has grown to a maximum and decays further downstream. An increase in formation length is also linked to a decrease in the streamwise normal Re stress [11, 12]. Regarding the far wake of flatback airfoils with TE devices, a similarity parameter based on geometrical characteristics of the model was recently discovered [13].

The vortex shedding at the TE of flatback airfoils at high chord Reynolds numbers ( $1.5e6 < Re_c < 3e6$ ) occurs at  $St \approx 0.24$  based on the free stream velocity and the TE height [13-16], while lower  $St$  values have been observed at lower  $Re_c$  numbers [17].  $St$  is increased with the various TE devices and it was recently found that the concept of a universal  $St^*$  number as introduced by Roshko [12, 18] also holds for various TE devices [13].

Combining the findings of various relevant studies, it can be said that TE drag reduction devices extend the vortex formation length at the wake of the blunt TE, thus increasing base pressure and  $St$  while reducing the flow fluctuations. In other words, the effect of the various devices is to transform the costly (in terms of drag) slow and large flow variations caused by bluff body vortex shedding into smaller, quicker variations that result in lower drag values.

Studies on flatback airfoils [4, 19] have shown that devices such as a Splitter plate, a Cavity or an Offset Cavity can achieve drag reduction up to 50%, for a small reduction in lift. Other devices have also performed well, such as a TE wedge, a Stepped Afterbody, a Ventilated Cavity, a Square Wave TE or M-shaped TE serrations [13, 20-22], but a single device has yet to emerge as the obvious choice for all cases, which suggest

more research is required. Regarding the length of the drag reduction devices it has been found that there is a critical length ( $\sim 0.5h$ , where  $h$  is the TE height) below which they become ineffective [4].

Drag reduction devices also affect lift, although not as dramatically as they affect drag [4]. As they extend downstream of the wing TE, parallel to its chord, they reduce the effective camber of the airfoil resulting in lower  $C_l$  values. The Splitter plate has a less pronounced effect on lift mainly because it is immersed in separated flow [19]. This is also the reason why serrations were found to have minimal effect on a single splitter plate, but improved the performance of the double splitter plate (Offset Cavity). Drag reduction devices attached to the TE of flatback airfoils can also reduce the noise generated in that region [23]. It is noted, however, that noise reduction is out of the scope of the present study.

## IV. Experimental Set up

### A. Wind tunnel and airfoil model

A 30% thick FB airfoil with a 10.6% thick TE (LI30-FB10, see Figure 1, left) was tested experimentally at  $Re_c = 1.5e6$ . The FB airfoil was generated from an airfoil with sharp TE of the same thickness (LI30) by adding thickness to the airfoil camber line gradually from  $x/c=0.4$  so that at the TE the added thickness is  $0.1c$ . The original LI30 was designed for use on a Low Induction Rotor (LIR) [24].

All experiments were performed at the small test section (1.4m×1.8m, height × width) of the National Technical University of Athens (NTUA) wind tunnel, where the turbulence intensity is  $\leq 0.2\%$ . A schematic view of the test set up is given in Figure 2. The wing spanned the test section vertically and fences were used in order to minimize the effect of the wind tunnel wall boundary layer. The model had a chord of  $c = 0.5m$  and the fences were 1m apart, setting the wing Aspect Ratio (AR) to 2.0.

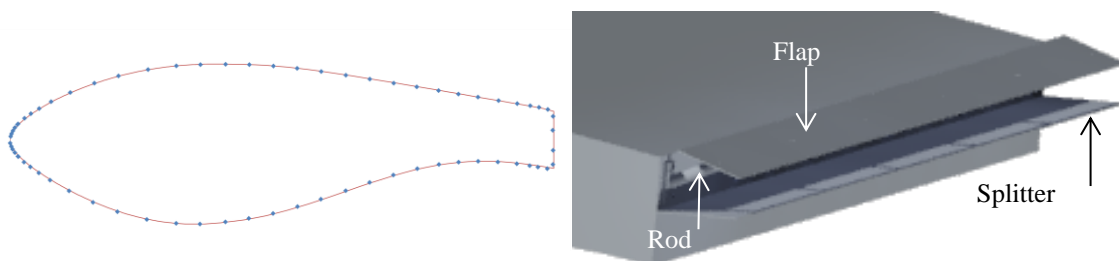


**Figure 1: (Left) The LI30-FB10 airfoil profile and the pressure tap positions. (Right) Drawing of the wing model with Flap + Splitter device, where one of the rods supporting the flap can be seen.**

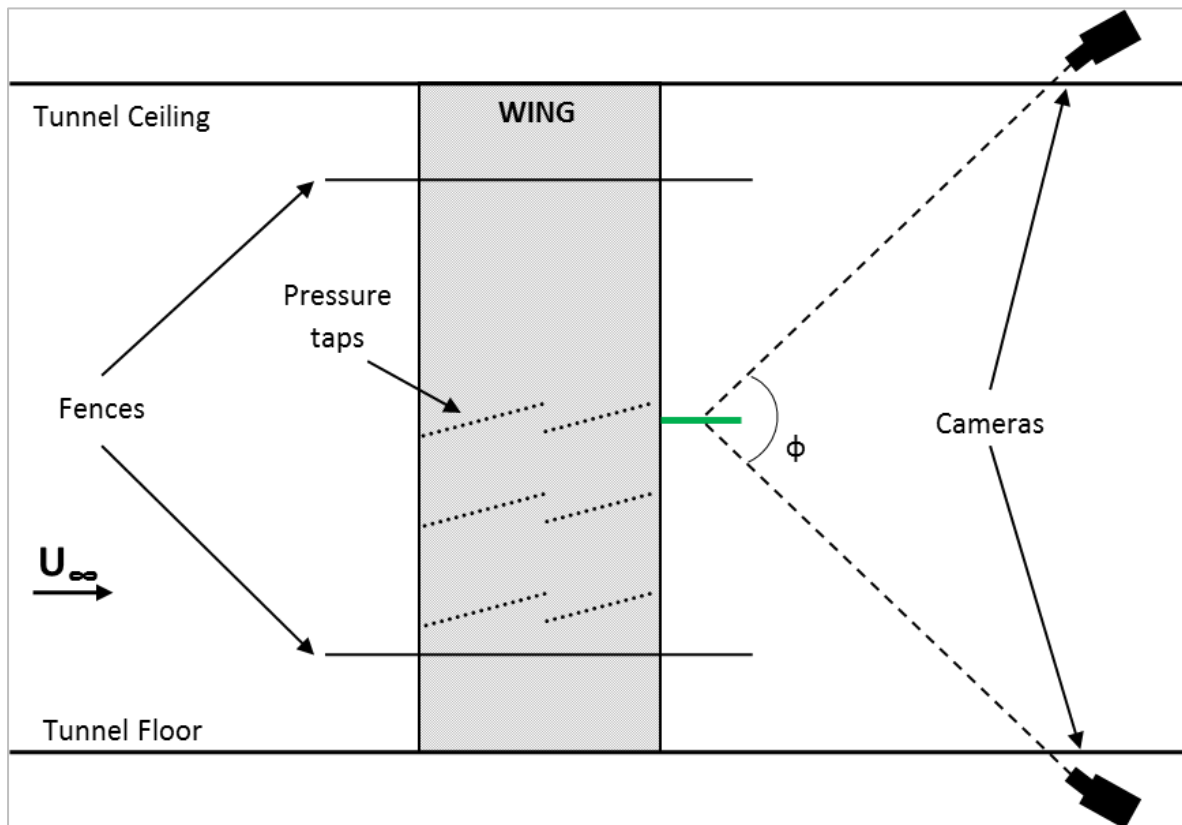


**Figure 2: Schematic planform view of the test set up showing the wing, the fences, the pressure taps and the Stereo PIV cameras. The measurement plane (green horizontal line) and the camera contained angle ( $\phi$ ) is also indicated.**

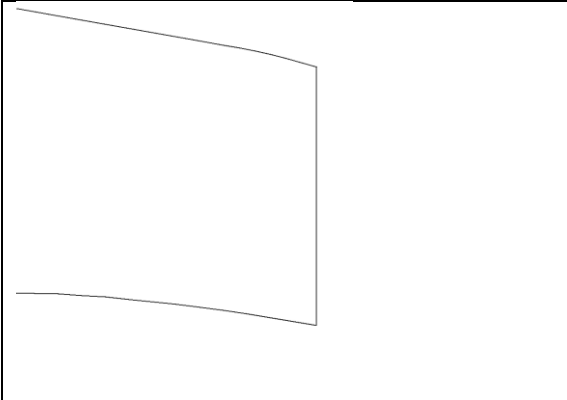
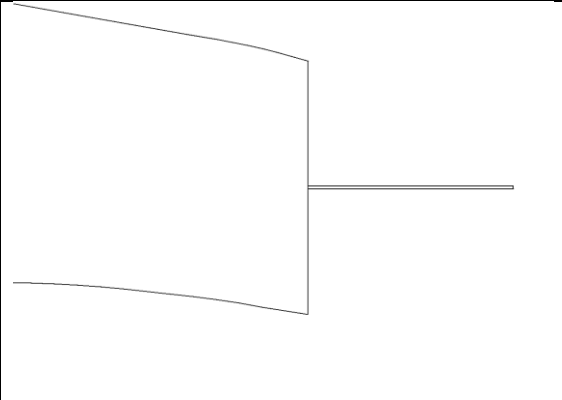
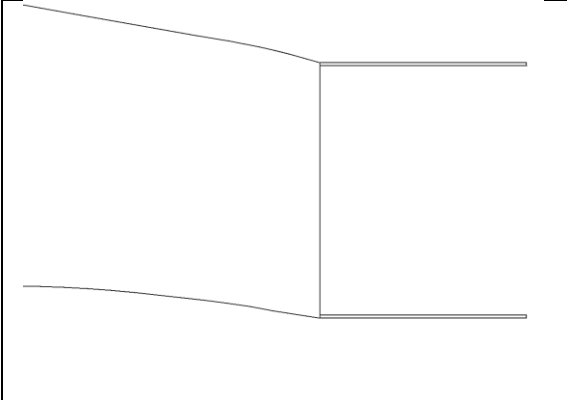
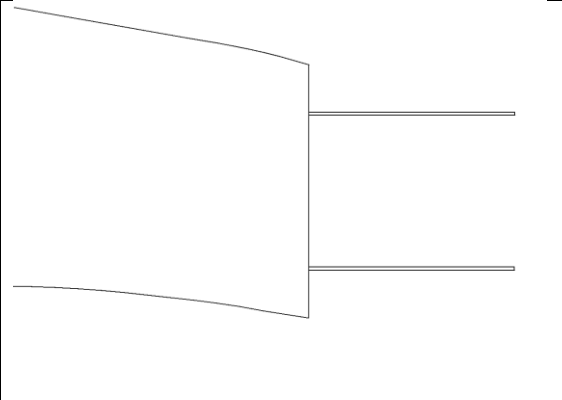
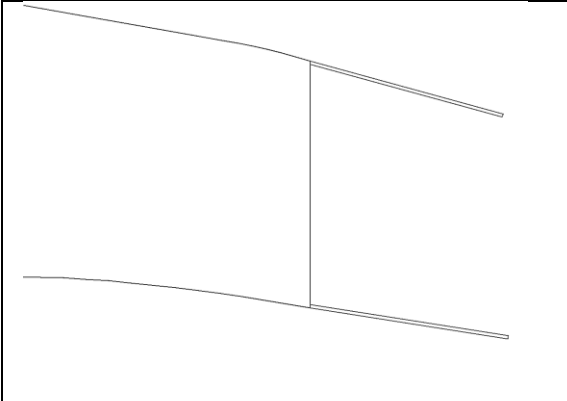
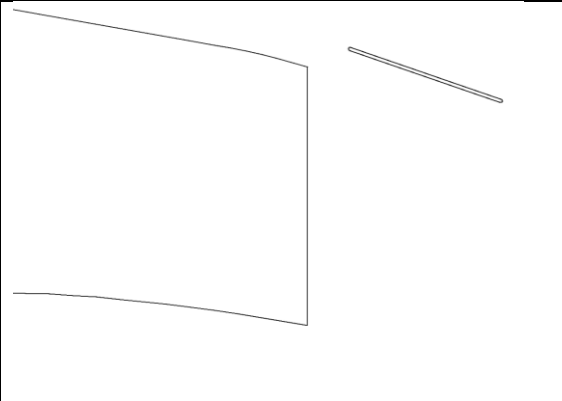
### **B. Drag Reduction Devices**

The drag reduction devices examined in the present study are categorized in two groups. The first group consists of three previously investigated devices (Splitter plate, Cavity and Offset Cavity), a variation of the Cavity (Extended Cavity) and a new Flap device, all five devices shown in Figure 3. The Extended Cavity is similar to the Cavity, but the plates follow the curvature of the airfoil sides at the TE. This means that they are neither parallel to the airfoil camber line nor to each other. The second group of devices is shown in Figure 4 and consists of four devices, which are combinations of the Flap with the Splitter plate and the lower part of the Cavity, the Offset Cavity and the Extended Cavity.

The Flap is a flat plate located at  $20^\circ$  with respect to the airfoil chord. Unlike usual TE airfoil slotted flaps, where the flap top side is fed with high speed flow from the airfoil lower side, in the present case the lower Flap

side is fed by the flow from the top airfoil side. To the best of the authors' knowledge such a device has not been previously tested on FB airfoils.

All devices were constructed by 2mm thick aluminum sheet. The Splitter, Cavity, Offset Cavity and Extended Cavity were 43mm long (or  $0.81h$ , where  $h = 53\text{mm}$  is the TE height). The Offset Cavity plates were located 10mm off the TE edges. The Flap was 33mm long or  $0.62h$ , its TE being at 40mm downstream of the airfoil TE. In the wind tunnel, the Flap was based on six support rods that were bolted on the wing TE with a spacing of 20cm along its span. A drawing of the wing model with the Flap + Splitter device is given in Figure 1 (right), where one of the rods can be seen.

	
Plane airfoil	Splitter
	
Cavity	Offset Cavity
	
Extended Cavity	Flap

**Figure 3: Detail of the FB airfoil trailing edge. 1<sup>st</sup> group of drag reduction devices.**



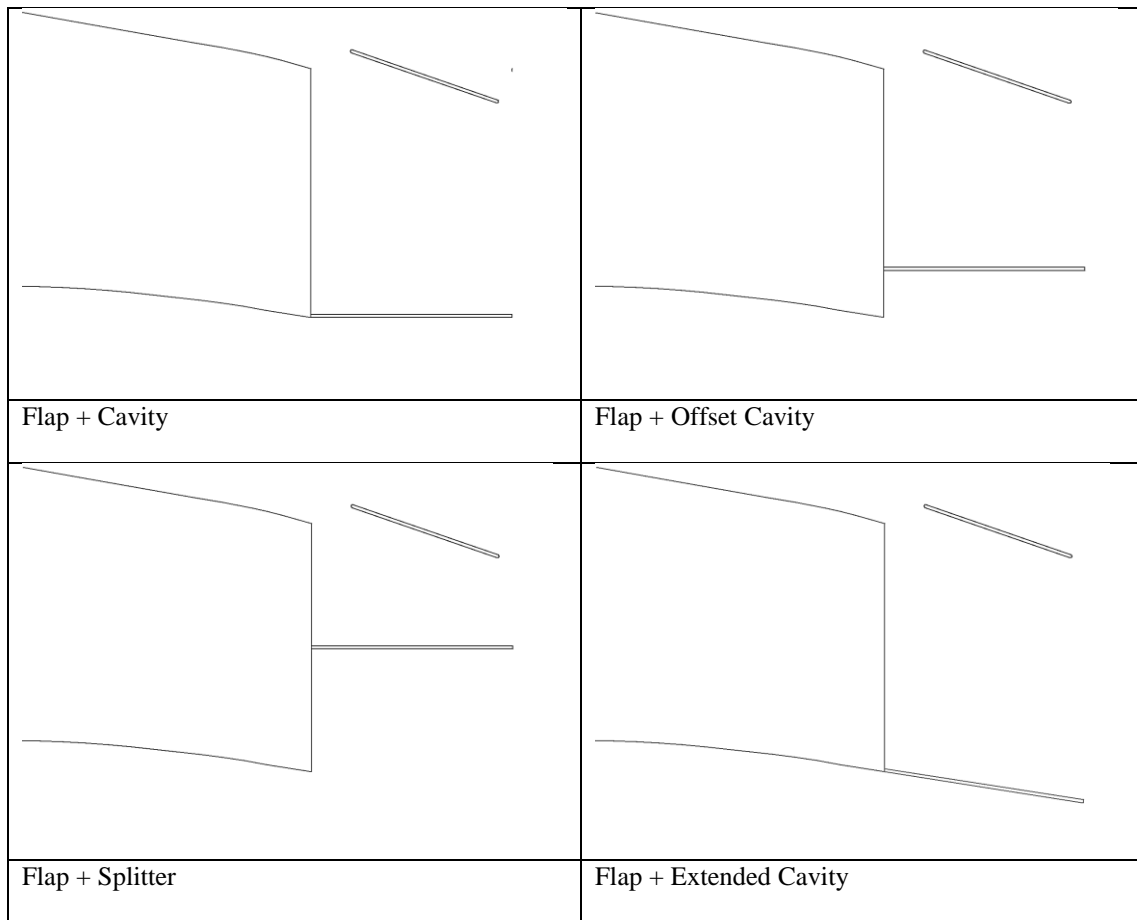


**Figure 4: Detail of the FB airfoil trailing edge. 2<sup>nd</sup> group of drag reduction devices.**

### C. Pressure Measurements

The wing model was equipped with three chordwise sets of pressure taps, at different spanwise locations. Data reported in this investigation concern the measurements from the taps located at the center of the wing span. In total 62 pressure taps were used, four of which were located at the wing TE. In addition, a wake rake was used to record the wake velocity. The rake consisted of 55 total pressure tubes and five static pressure tubes. It was positioned  $1.8c$  downstream of the wing TE and could move both in the spanwise direction and in the direction normal to the wing span. The drag was measured at the center of the wing span and, in the cases with a flap, between two consecutive support rods to avoid any interference. Four 32-channel MicroDaq Pressure Scanners (manufactured by Chell Instruments) were used to obtain 30sec long measurements at 40Hz and 50Hz.

The lift and pressure drag coefficients were computed from the pressure distribution around the airfoil. The wake rake drag coefficient was calculated from the wake pressure distribution according to [25]. The reported drag coefficient value is the rake drag until  $\alpha_{Cl_{max}}$  and the pressure drag for higher angles of attack. In some cases where the wake was not entirely captured by the wake rake, no drag or L/D value is reported. Standard

wind tunnel corrections were applied to the measured data [25], as they have been found to be valid for thick flatback airfoils [26]. Free transition measurements are reported in this investigation, unless otherwise stated.

#### **D. Stereo PIV Measurements**

All measurements concern a plane normal to the wing axis at the center of its span. The cameras were located above and below the test section, 85cm or  $1.7c$  downstream of the wing TE. All Stereo PIV measurements were taken with the wing at  $\alpha = -0.6^\circ$  and at  $Re_c = 1.5e6$ . For each case 1000 snapshots were taken and the results presented here are the averaged data.

A 200mJ Nd:YAG PIV laser (Litron Lasers) with dual cavities was used to create a 1.8mm thick light sheet at the measurement plane. The flow was seeded with oil droplets of  $1\mu\text{m}$  mean diameter created by a commercial generator (TSI model 9307). Two 12-bit TSI Powerview Plus™ 4MP Cameras with Sigma 150mm f/2.8 lenses were used to obtain the data. The camera contained angle ( $\varphi$  in Figure 2) was  $\varphi \approx 88^\circ$ .

#### ***Pulse separation time***

In Stereo PIV experiments a compromise is necessary between a small pulse separation time that will minimize errors associated with flow acceleration and curvature effects and a large separation time that will result in a sufficiently high dynamic range and acceptable relevant measurement error. In the present case a pulse separation time of 8  $\mu\text{sec}$  was used as higher values would increase the measurement noise and make peak detection harder. For all planes the number of spurious vectors was always below 5% and spurious vectors were replaced using a  $3 \times 3$  vector local mean. The particle displacement was in all cases less than  $1/4$  of the  $32 \times 32\text{px}$  final interrogation area, which was  $1.8 \times 1.8\text{mm}$  in actual dimensions.

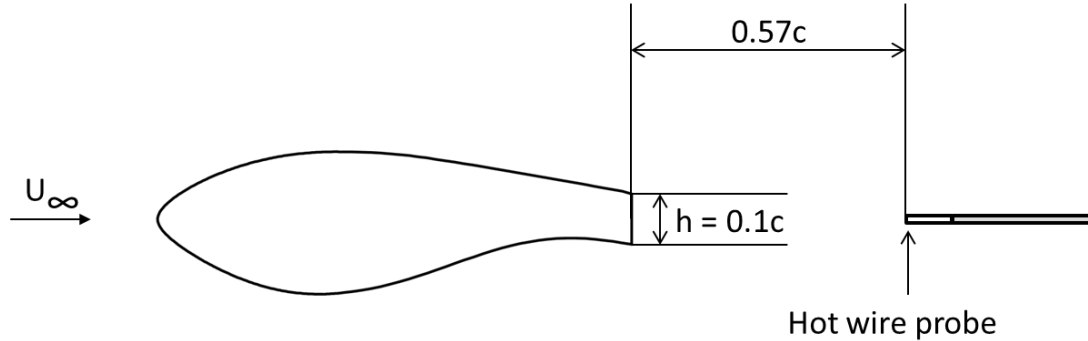
#### **Image Processing**

Image processing was performed using the Insight 4G (TSI) software. In pre-processing a background reflection image was subtracted from the original images to remove unwanted reflections. In processing, the overlap between interrogation areas was set to 50% and a Gaussian peak estimator was used.

#### **E. Hot Wire Measurements**

Hot wire measurements were performed at the wake of the flatback airfoil with and without TE drag reduction devices. The hot wire was located  $0.57c$  downstream of the wing TE, at the center of the wing TE height with the wing located at  $\alpha = 0^\circ$ , see Figure 5. The spanwise location of the probe was the same as the Stereo PIV

measurement plane, i.e. at the center of the wing span. A single wire probe was used to examine the spectral content of the wake. The sampling rate was 4000HZ and the sample time was 8.2 sec.



**Figure 5: Hot wire probe location with respect to the wing**

## F. Uncertainty Analysis

The model angle was set with  $0.2^\circ$  accuracy. The 95% confidence interval for the lift and drag values are 1% and 4%, respectively. The relatively high value of uncertainty for the drag value is due to the unsteadiness of the flow and the vibrations of some of the rake tubes. For clarity the 4% error bars are only drawn in Figure 8 on the plane airfoil data. For the examined hot wire samples, the frequency step was 1.95Hz.

### 1. Stereo PIV

Under optimal conditions the minimum displacement that can be accurately estimated using PIV is 0.1px [27, 28]. The corresponding minimum resolvable velocity for a pulse separation time of 8  $\mu\text{sec}$  was  $U_{res} = 0.7\text{m/s}$  or 1.5% of  $U_\infty$ . Any estimated velocity lower than this value is not reliable.

In Figure 6, the measured time averaged streamwise velocity value for different sample sizes is plotted. The data concern a point right after the plane wing TE, i.e. a point in the most unsteady region of the flow. A horizontal solid black line is drawn at the velocity value based on the maximum number of snapshots (1000). Above and below this line, two parallel dotted lines are drawn at a distance equal to the minimum resolvable velocity ( $U_{res} = 0.7\text{m/s}$ ). The 95% confidence interval is given with a blue dashed curved. This suggests that for 1000 snapshots, the 95% confidence interval is comparable to  $U_{res}$ .

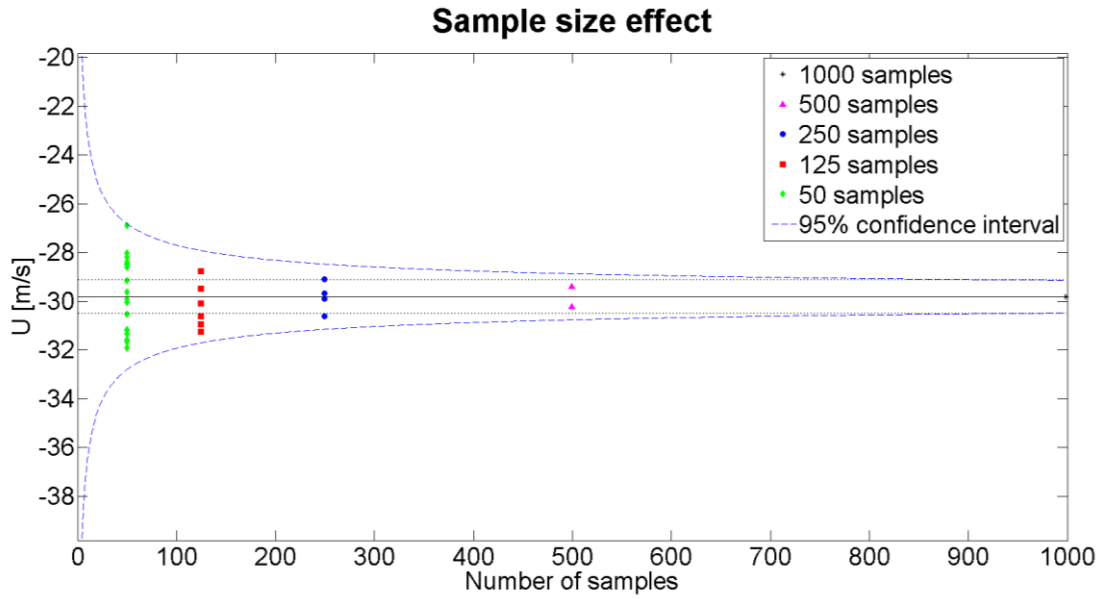


**Figure 6: Sample size effect on the streamwise velocity component (U) at a point right after the plane wing TE.**

## V. Results and Discussion

### A. Force Coefficient Polars

The flatback airfoil examined in the present study is based on a LIR airfoil [24]. The Low Induction Rotor is the concept of a larger rotor designed with low lift airfoils to achieve increased energy capture and decreased levelised cost of energy compared to the traditional wind turbine rotor designs. Keeping this in mind, the discussion of the results in the present paper examines lift, drag and L/D, even though lift would be the main factor for a thick flatback airfoil located at the inboard part of a traditionally designed rotor.

#### 2. 1<sup>st</sup> Group of Drag Reduction Devices

The performance of the first set of drag reduction devices (Splitter, Cavity, Extended Cavity, Offset Cavity and Flap) compared to the plane airfoil is given in Figure 7 ( $C_l$  vs.  $\alpha$ ), Figure 8 ( $C_d$  vs.  $\alpha$ ), Figure 9 (L/D vs.  $C_l$ ). For the Low Induction Rotor, the design  $C_l$  is 0.8 [24], so, in order to examine the performance of each device at that  $C_l$  region, L/D is plotted against  $C_l$  rather than  $\alpha$ .

All devices resulted in lower drag values at angles of attack  $\alpha < 12^\circ$  compared to the plane airfoil. The biggest drag reduction (~50%) was achieved by the Splitter, the Offset Cavity and the Flap. It is noted that

although the reduction for the three devices is of the same magnitude, the flow mechanism through which this reduction is achieved is different, as discussed in Section C. Stereo PIV results.

In terms of lift in the pre-stall region, only the Extended Cavity offered improvements, while the Flap had similar performance to the plane airfoil. All other devices resulted in lower  $C_l$  values. Stall was delayed by  $2^\circ$  when the Extended Cavity or Cavity was used. The Flap delayed stall by  $1^\circ$ , whereas the Splitter and the Offset Cavity did not affect  $\alpha_{Cl_{max}}$ .

In terms of  $L/D$ , the Offset Cavity, the Splitter and the Flap outperform the plane airfoil in the region  $0.1 < C_l < 1.6$ . All three devices almost double  $L/D$  at the design  $C_l$  region ( $C_l = 0.8$ ), while the Offset Cavity offers the highest  $L/D$  value ( $L/D = 69.7$ ). Devices attached right on the blunt TE edges (the Cavity and the Extended Cavity) only offer small improvements compared to the plane airfoil from  $C_l \geq 0.5$  up to stall.

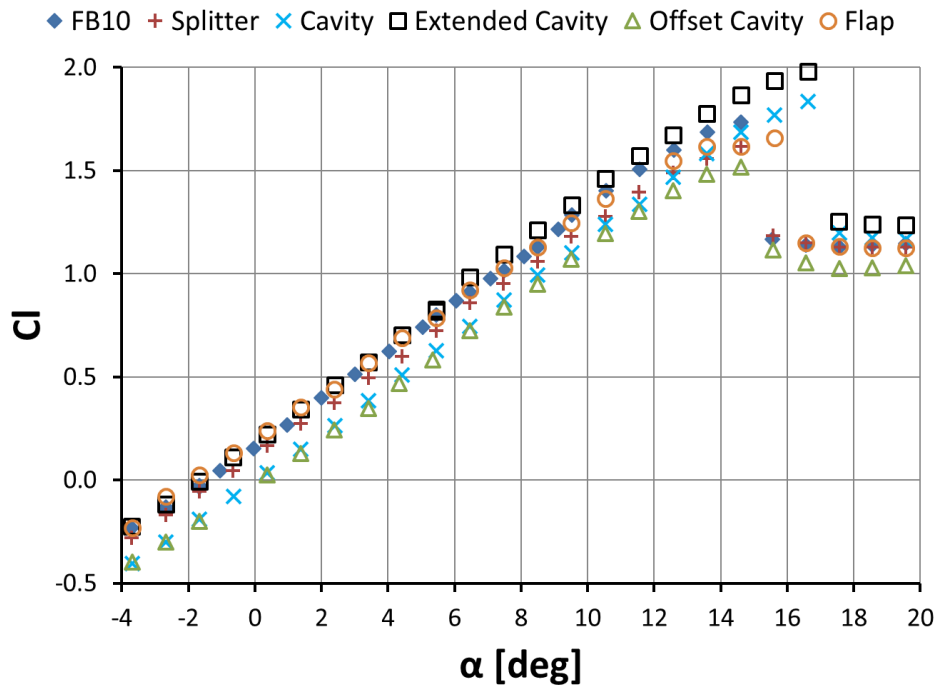


**Figure 7: Lift coefficient variation with angle of attack. Comparison between the plane airfoil and the airfoil with Splitter, Cavity, Extended Cavity, Offset Cavity and Flap**

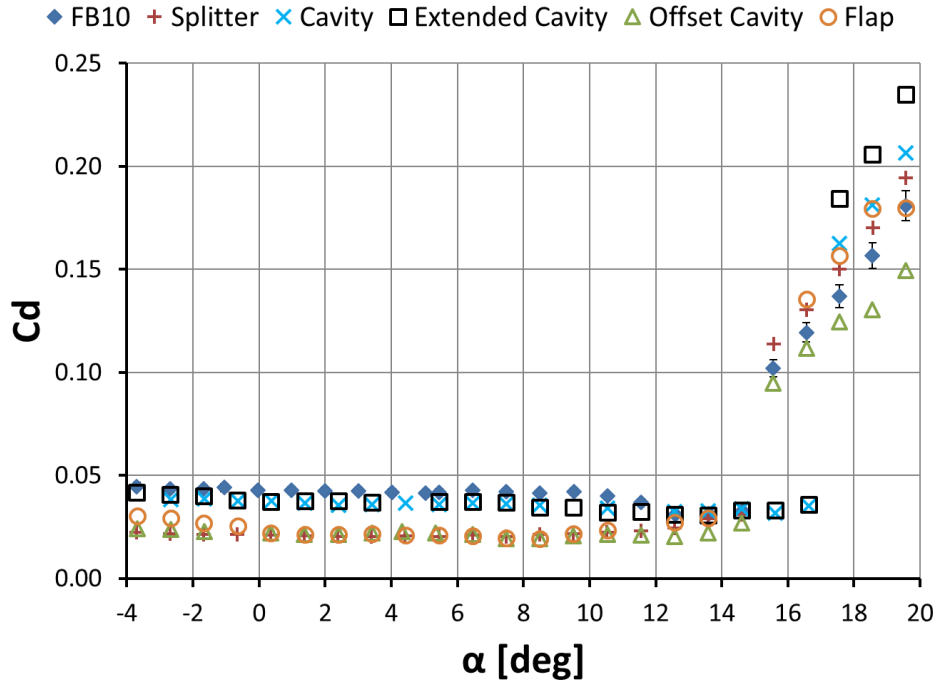


Figure 8: Drag coefficient variation with angle of attack. Comparison between the plane airfoil and the airfoil with Splitter, Cavity, Extended Cavity, Offset Cavity and Flap

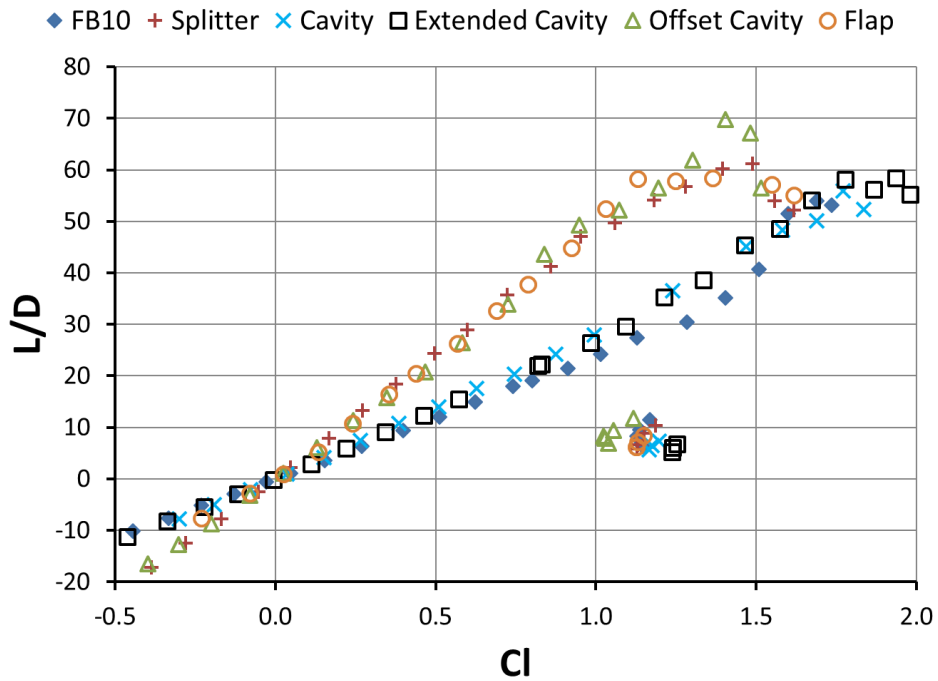


Figure 9:  $L/D$  variation with lift coefficient. Comparison between the plane airfoil and the airfoil with Splitter, Cavity, Extended Cavity, Offset Cavity and Flap

The best performing device among those of the 1<sup>st</sup> group is the Offset Cavity. Both the Splitter and the Flap also show promising results, increasing L/D significantly in the design Cl region. It is highlighted here that although their performance is similar in terms of L/D this is achieved in different ways, as the Flap mainly affects drag, while the splitter reduces both lift and drag.

### 3. 2<sup>nd</sup> Group of Drag Reduction Devices

The Flap was also tested in combination with the Splitter, Cavity, Extended Cavity and Offset Cavity, as shown in Figure 4. The Lift, Drag and L/D variation are given in Figure 10, Figure 11 and Figure 12, respectively.

Preliminary results showed that the Flap + Cavity and the Flap + Extended Cavity do not outperform the simple Flap device in terms of L/D, but higher Cl values can be achieved. The Flap + Splitter and Flap + Offset Cavity combinations provide similar results in terms of L/D, with the former providing higher Cl values and the latter lower Cd values.

The Flap + Offset Cavity combination performs better than any of the devices examined in this investigation in terms of L/D, especially in the design Cl region. The drag reduction benefit is similar or better than the simple Offset Cavity device and it is accompanied by a beneficial Cl increase at small angles of attack.

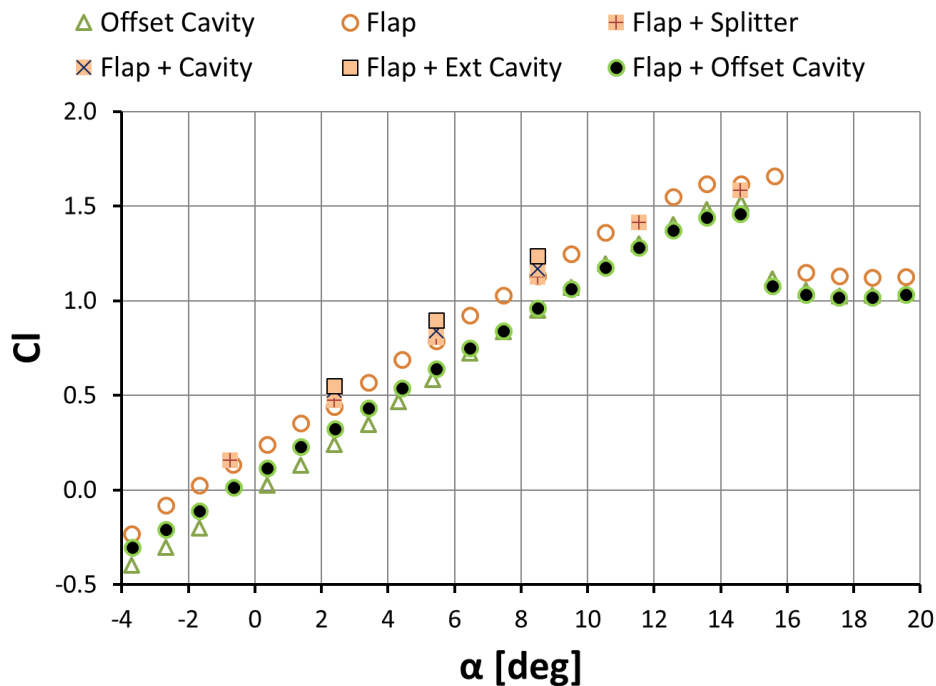


**Figure 10: Lift coefficient variation with angle of attack. Comparison between the airfoil with Offset Cavity, Flap, Flap + Splitter, Flap + Cavity, Flap + Extended Cavity and Flap + Offset Cavity**

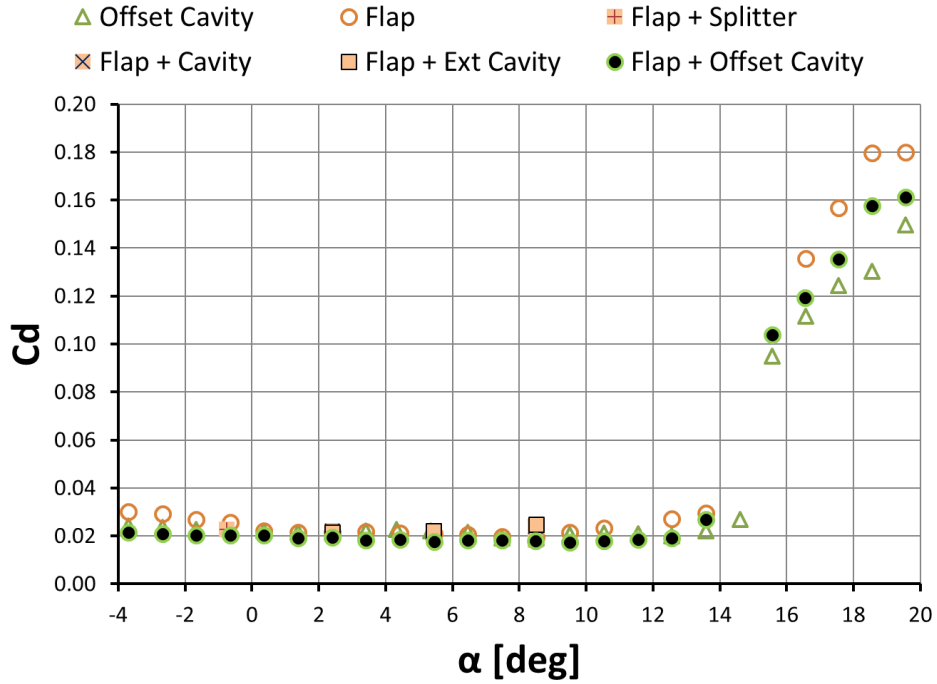


Figure 11: Drag coefficient variation with angle of attack. Comparison between the airfoil with Offset Cavity, Flap, Flap + Splitter, Flap + Cavity, Flap + Extended Cavity and Flap + Offset Cavity

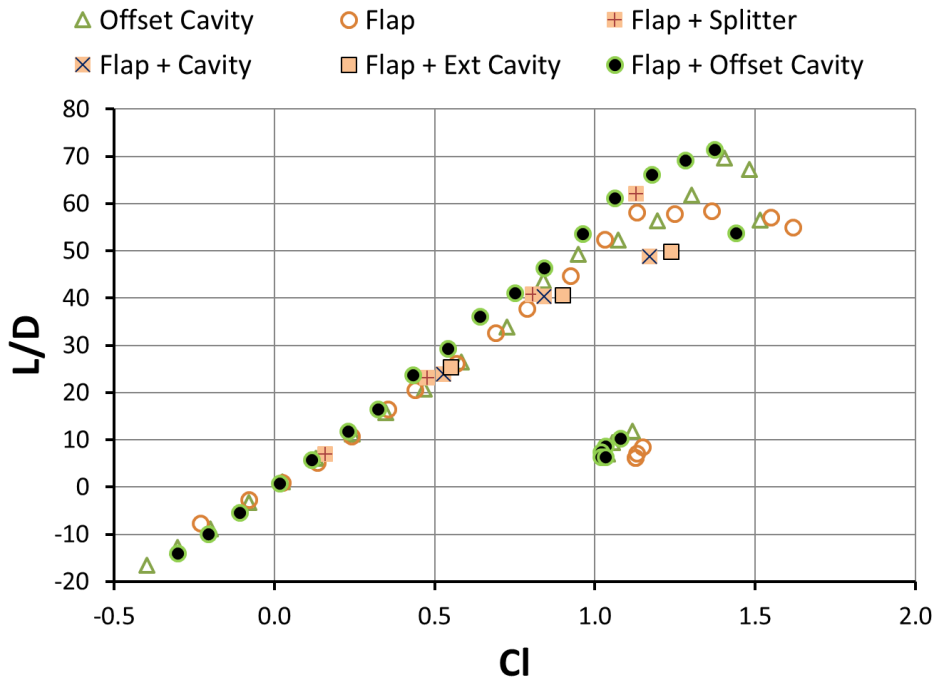


Figure 12: L/D variation with lift coefficient. Comparison between the airfoil with Offset Cavity, Flap, Flap + Splitter, Flap + Cavity, Flap + Extended Cavity and Flap + Offset Cavity



Although the focus of this study is the pre-stall performance of the airfoil with and without the TE devices, it is worth noting that the plane airfoil experienced 3D separation of the Stall Cell type (see Figure 13) and that none of the devices changed the SC type, despite delaying SC formation. SCs are large scale 3D structures of separated flow [29, 30] that appear on the suction side of airfoils experiencing TE type stall [31] at angles of attack near stall.



**Figure 13: Flow visualization on the plane airfoil suction side,  $\alpha = 15^\circ$ ,  $Re_c = 1.5e6$ . The flow is from top to bottom and gravity is from right to left, as the model was located vertically in the wind tunnel. Thin white lines highlight the wing LE and TE. Reflection from the UV light used to take the photograph is visible close to the LE. Tapes were used to cover the pressure taps during the flow visualization tests.**

## B. Pressure Distribution

The effect of each drag reduction device on the pressure distribution around the airfoil is examined in this section. It is observed that all devices result in higher base pressure values and that the reduction in  $C_d$  is almost linearly linked to the base pressure (Figure 14).

The TE devices effect is not limited to the TE region, as the pressure is affected all around the airfoil, see Figure 15. The Splitter and the Offset Cavity have a more significant overall effect which explains the significant drop in  $C_l$  for these devices. Adding the Flap to the Offset Cavity or the plane airfoil appears to mainly increase base pressure at the wing TE with minor effects on the pressure distribution away from the TE region.

All devices increase the pressure difference between the suction peak and the pressure at the blunt TE, which could result in increased roughness sensitivity for the airfoil. Unfortunately, no fixed transition measurements

were performed for the airfoils with the TE devices so further investigation is required. The performance of the plane airfoil, however, was virtually unaffected by fixing the transition by means of a zigzag tape located at 3% chord on both sides of the airfoil.

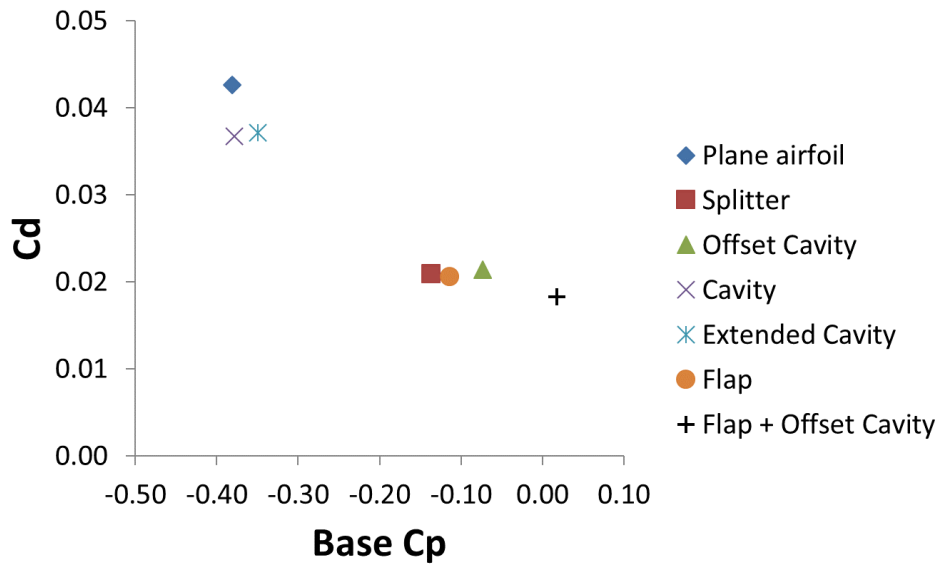


**Figure 14: Drag coefficient variation with base pressure coefficient at  $\alpha = 6.4^\circ$ ,  $Re_c = 1.5e6$ , for the plane airfoil and the airfoil with Splitter, Offset Cavity, Cavity, Extended Cavity, Flap and Flap with Offset Cavity**

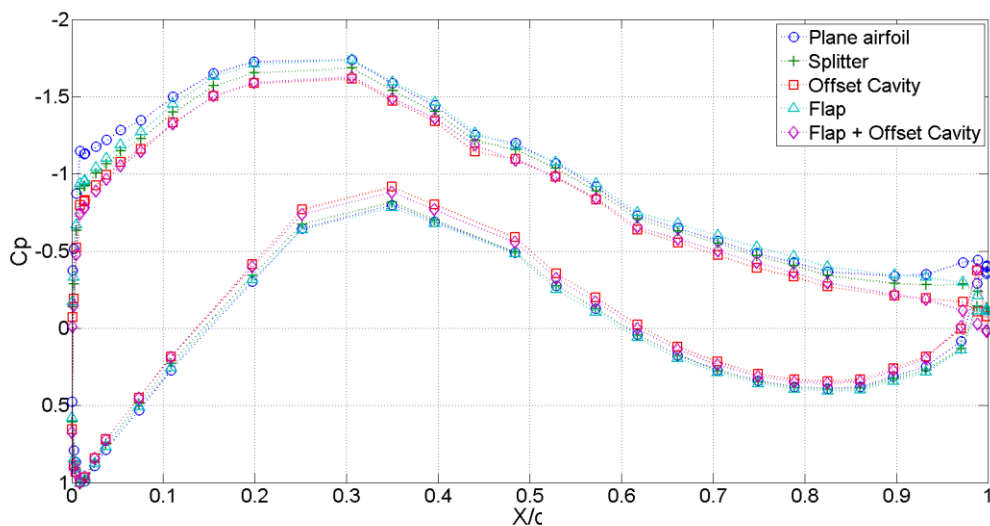


**Figure 15: Pressure coefficient distribution along the wing chord at  $\alpha = 6.4^\circ$ ,  $Re_c = 1.5e6$ , for the plane airfoil and the airfoil with Splitter, Offset Cavity, Flap and Flap with Offset Cavity**

### C. Stereo PIV results

The plane airfoil and the four best performing configurations (Offset Cavity, Splitter, Flap, Flap + Offset Cavity) were examined using Stereo PIV. The results are presented in contour plots in the following manner. The flow is from left to right and the center of the TE is at  $X/c = 1$ ,  $Y/c = 0$ . An outline of the wing TE and the TE device used each time is also shown.

As the laser source was located outside the test section, at the side of the airfoil top surface, the drag reduction devices shadowed part of the measurement plane. The measurement plane for each case is shown in Figure 16. The shadowed part along with areas affected by reflections has been masked out. All data have been non-dimensionalized with  $U_\infty$  and the wing chord ( $c = 0.5\text{m}$ ).

#### 1. Mean Flow

Figure 17 and Figure 18 show the mean streamwise velocity and spanwise vorticity contours for each case, respectively. In Figure 17 streamlines are also given, based on which the vortex centers and the saddle point in the wake are identified. As a reference between the various contours, the vortex centers and the saddle point are given in all plots.

All devices appear to move the saddle point and the vortex centers downstream compared to the plain airfoil case. The vortex centers cannot be identified in the Flap case, as they are probably in the shadowed region, where no data are available.

It is noted that the highest vorticity values correspond to the two shear layers that leave from the wing surfaces and not the vortex centers. For the Flap cases two distinct regions of high negative vorticity are observed, one corresponding to the Flap wake and one to the top wake vortex. The Flap + Offset Cavity case is the only case where the center of the lower vortex is further downstream than the top one.

For both flap cases, no reversed flow is observed in the vicinity of the flap, at least in the region where data are available, suggesting that the flap is well aligned with the local flow for the examined angle of attack.

#### 2. Turbulence characteristics

In the  $\overline{u'v'}$  contours for the plane airfoil (Figure 19) two large regions of high positive (top) and negative (bottom) values are observed. These indicate the size and intensity of the shear layers that form downstream of the wing TE. Upstream of these two regions two smaller regions of opposite  $\overline{u'v'}$  sign appear, also upstream of the vortices centers. The overall picture is very similar to the high speed 2D PIV results presented in [13]. The  $\overline{u'v'}$  pattern for the Offset Cavity is also similar, suggesting that the same flow pattern appears. The only

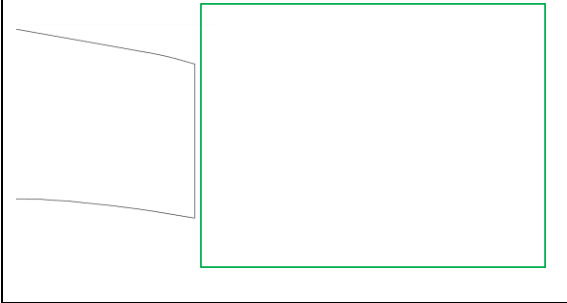
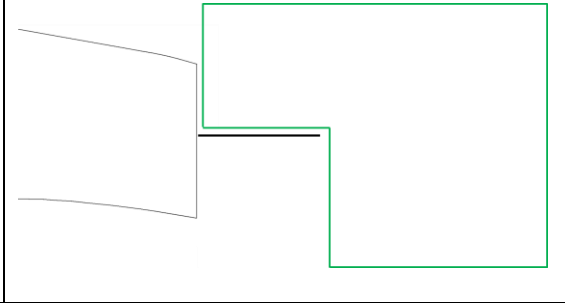
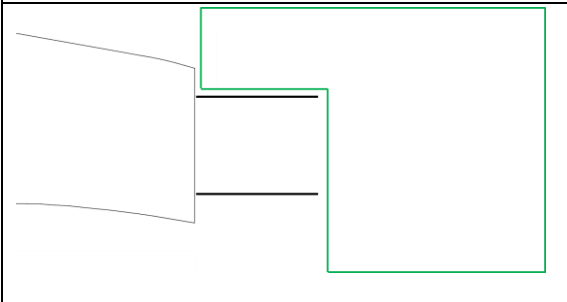
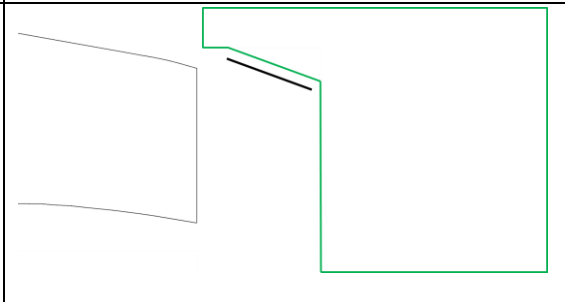
difference is in size and Re stress magnitude, as the flow pattern appears to scale with the cavity height rather than TE height.

In the Splitter case the two large regions indicating the two shear layers that meet are also observed, but the smaller regions of opposite sign are not, suggesting a different flow mechanism in the wake. The Splitter is too short to completely prevent vortex shedding [12], but it does delay it until further downstream.

In the Flap case the lower shear layer is much more intense than the top which is affected by the presence of the flap. When the Offset Cavity is added to the Flap, the  $\overline{u'v'}$  intensity drops significantly for both shear layers suggesting a much more stable flow.

In Figure 20 the  $\overline{u'u'}$  Re stress contours are presented. Regions of high  $\overline{u'u'}$  values can be considered as indicators of the regions where the shear layers move in the vertical direction. In the plane airfoil case two areas of high  $\overline{u'u'}$  values appear, which correspond to the regions where high speed flow from outside the wing wake is fed into it as the vortices are shed from each side, in an alternating manner. Each time a vortex leaves the wing TE, it moves towards the wing centerline and pulls in high speed flow from outside the wake. At the same time it induces velocities of opposite sign at the other side of the TE. Through this mechanism the two regions of high  $\overline{u'u'}$  appear downstream of the vortex centers. For the Splitter, Offset Cavity and Flap cases the relevant  $\overline{u'u'}$  values are reduced and even more so for the Flap + Offset Cavity case.

High  $\overline{v'v'}$  values indicate regions where the formed vortices move in the streamwise direction. Consider a point along the path of the shed vortices and let's accept for simplicity that this path is parallel to the free stream. The flow variation in the vertical direction at this point, as the vortices travel through it, will be large and high  $\overline{v'v'}$  values will be recorded. The region of intense  $\overline{v'v'}$  values is large for the plane airfoil case. The  $\overline{v'v'}$  contour is very similar for the Offset Cavity, but the region is now smaller, again suggesting scaling with the cavity height. The  $\overline{v'v'}$  variations are small for the Splitter and start further downstream, indicating how the device delays the shear layer roll up. For the Flap case high  $\overline{v'v'}$  values appear at the lower part of the flow, corresponding to the vortex shed from the lower part of the TE. The Flap + Offset cavity is the device with the lowest variation in the vertical direction with values almost an order of magnitude smaller than the plane airfoil.

	
Plane airfoil	Splitter
	
Offset Cavity	All the Flap cases

**Figure 16: Stereo PIV measurement window for each case**

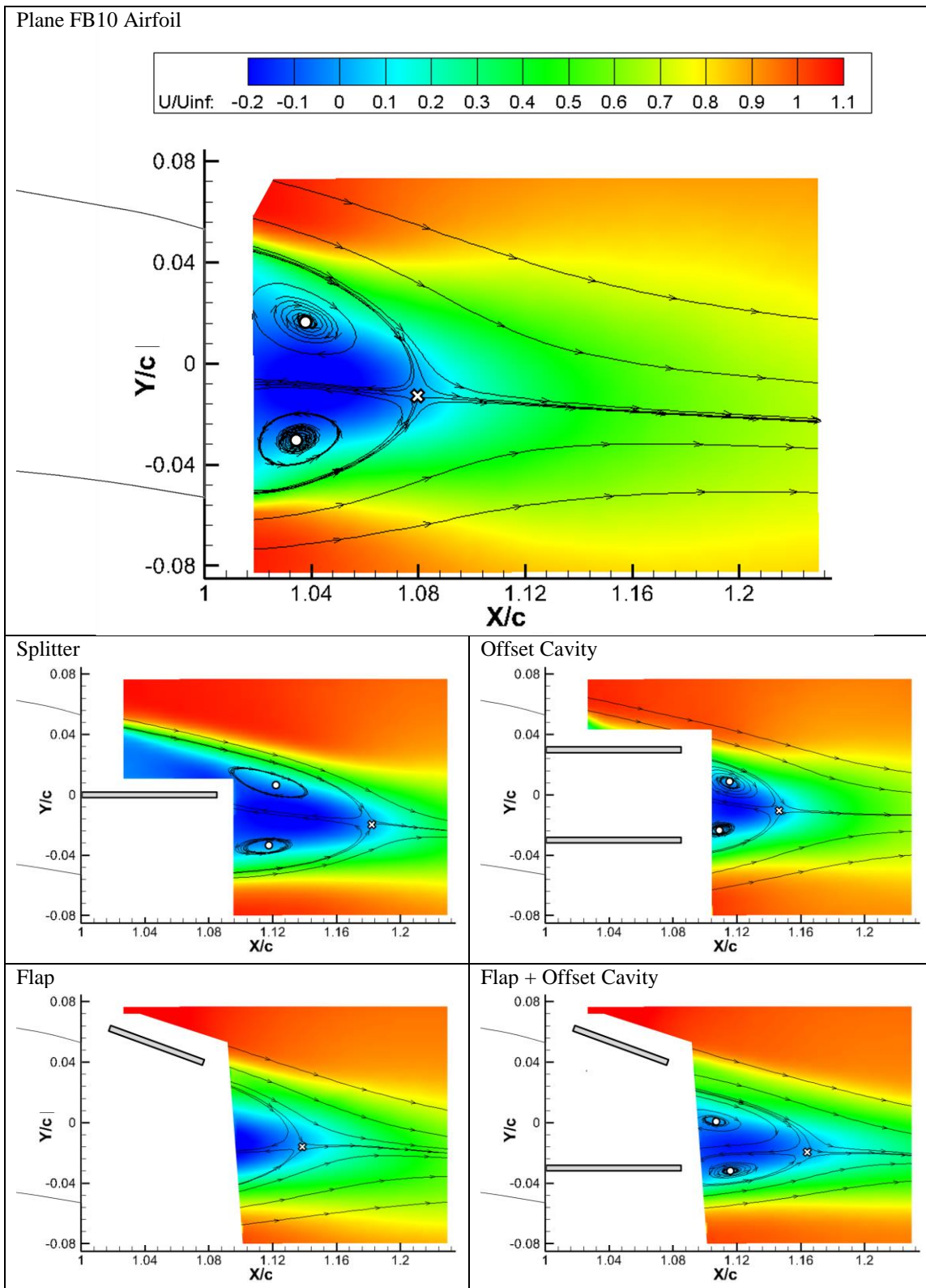


Figure 17: Streamwise velocity contours and in plane streamlines. The location of the saddle point in the wake is also indicated. The circles and the “X” sign indicate the vortex centers and the saddle point in the wake, respectively.

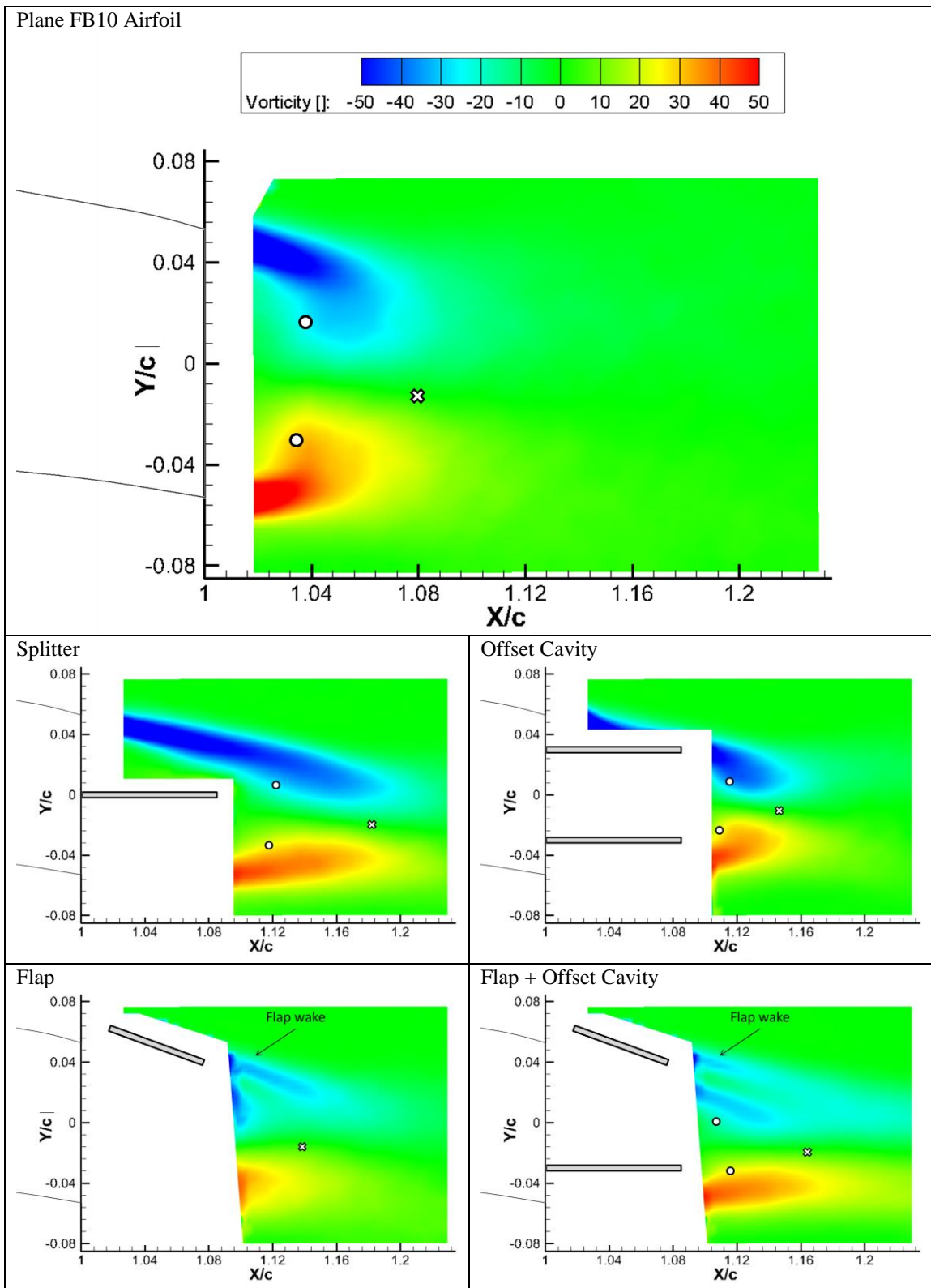


Figure 18: Spanwise vorticity contours. The circles and the “X” sign indicate the vortex centers and the saddle point in the wake, respectively.

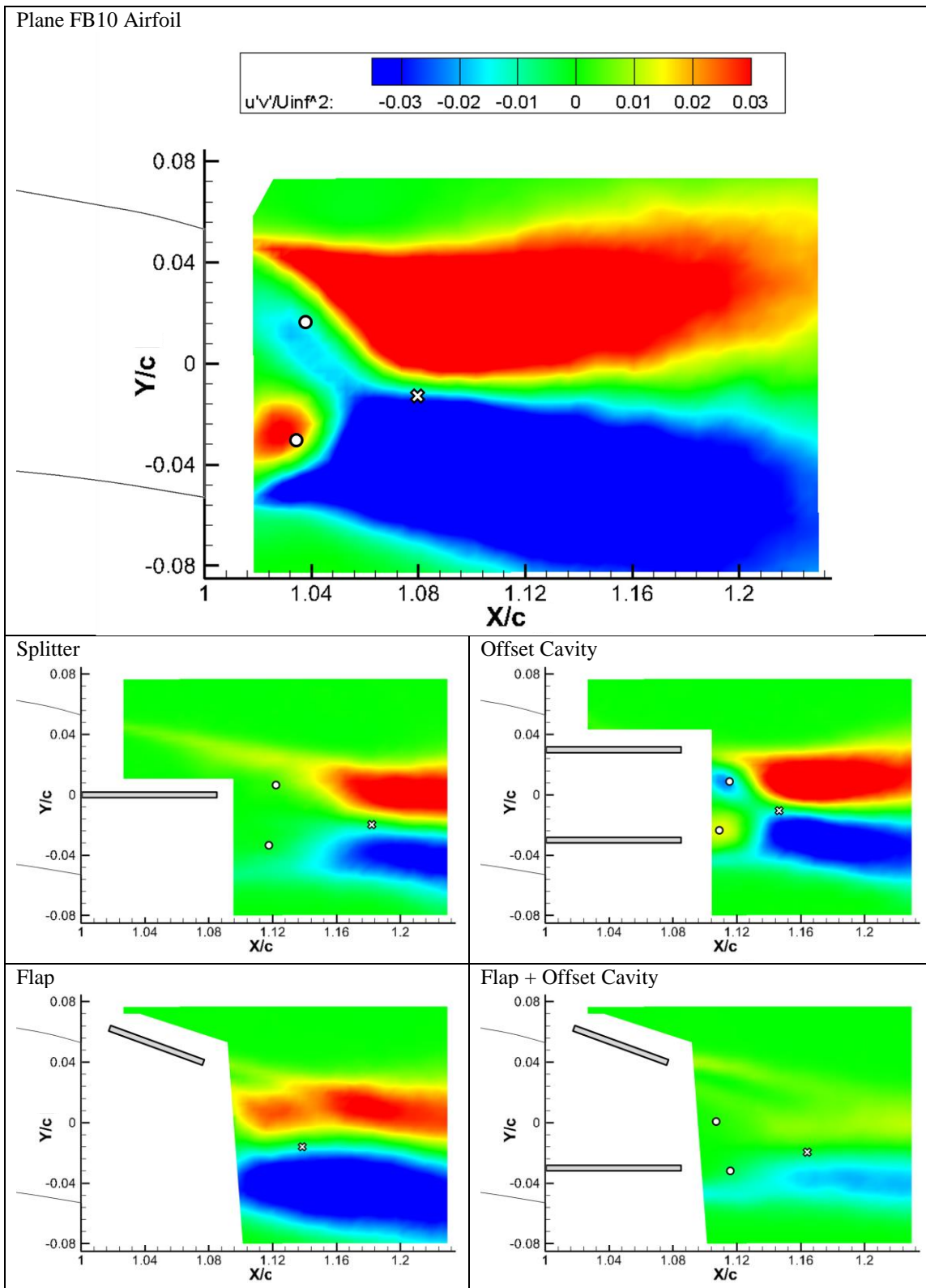


Figure 19:  $\overline{u'v'}$  shear Reynolds stress contours. The circles and the “X” sign indicate the vortex centers and the saddle point in the wake, respectively.



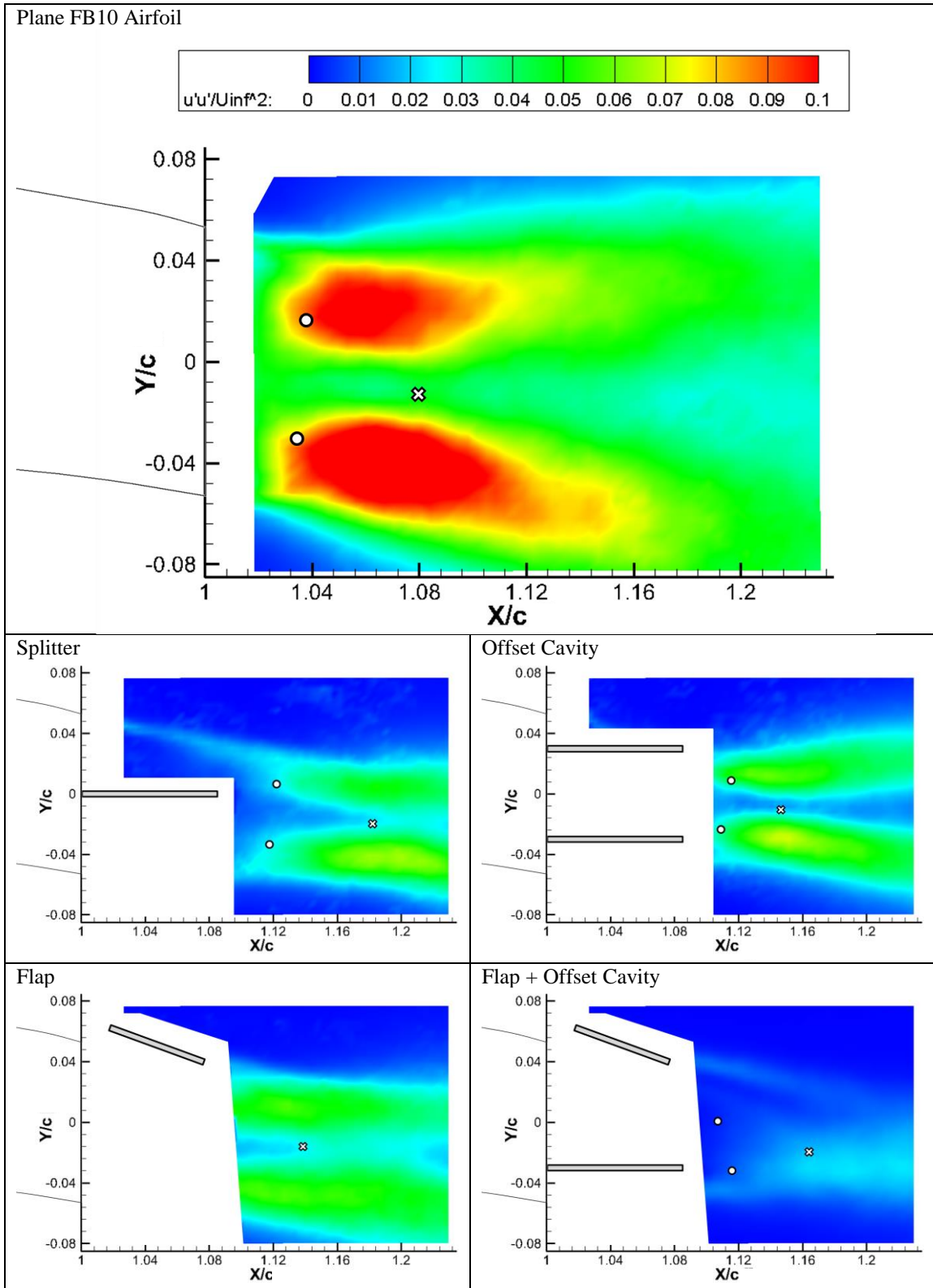


Figure 20:  $\overline{u'u'}$  normal Reynolds stress contours. The circles and the “X” sign indicate the vortex centers and the saddle point in the wake, respectively.

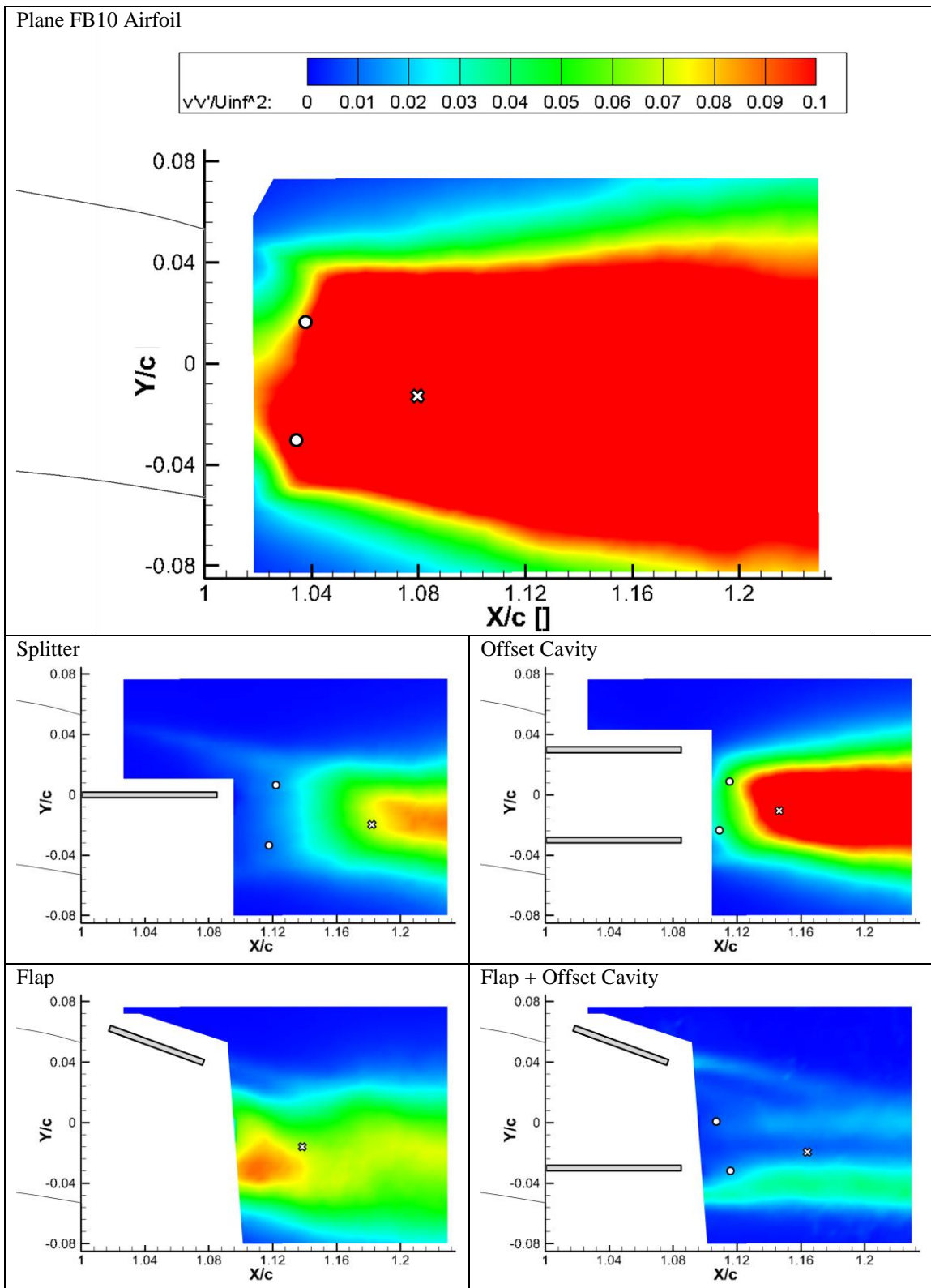


Figure 21:  $\overline{v'v'}$  normal Reynolds stress contours. The circles and the “X” sign indicate the vortex centers and the saddle point in the wake, respectively.

#### D. Hot wire results

The frequency spectrum from the hot wire measurements for the examined TE devices and the plane airfoil is given in Figure 22, while the dominant frequency for each case and the corresponding  $St$  are given in Table 1. The peak amplitude at the main shedding frequency is normalized with the peak amplitude of the plane airfoil and is also given in Table 1.

For the plane airfoil a peak is observed at 217Hz, while lower peaks appear at frequencies twice and three times the main frequency. A similar behavior is observed for all the examined devices, but the dominant frequency is always higher than that of the plane airfoil. For the Splitter and the Flap + Offset Cavity the third peak is hardly observable. For the Offset Cavity and the Flap, the peaks appear much sharper, suggesting that distinctly structured vortices pass through the point of measurement.

The only device that gives higher amplitude at the main frequency than the plane airfoil is the Flap (130% of the amplitude for the plane airfoil), while the Flap + Offset Cavity gives the lowest amplitude (16% of the amplitude for the plane airfoil). This is in agreement with the results from the Stereo PIV measurements, where significantly smaller flow variations were observed for the Flap + Offset Cavity than for any other device (see e.g. Figure 19). Excluding the main frequencies and their multitudes, the amplitude throughout the examined spectrum is smaller for all the devices compared to the plane airfoil, again in agreement with the Stereo PIV data.

	<b>Dominant frequency [Hz]</b>	<b>Normalized Peak Amplitude</b>	<b><math>St</math></b>
<b>Plane Airfoil</b>	217	1.00	0.24
<b>Splitter</b>	285	0.50	0.31
<b>Offset Cavity</b>	320	0.88	0.35
<b>Flap</b>	244	1.30	0.27
<b>Flap + Offset Cavity</b>	281	0.16	0.31

**Table 1: Dominant frequency, normalized peak amplitude and corresponding  $St$  for the examined TE devices and the plane airfoil**

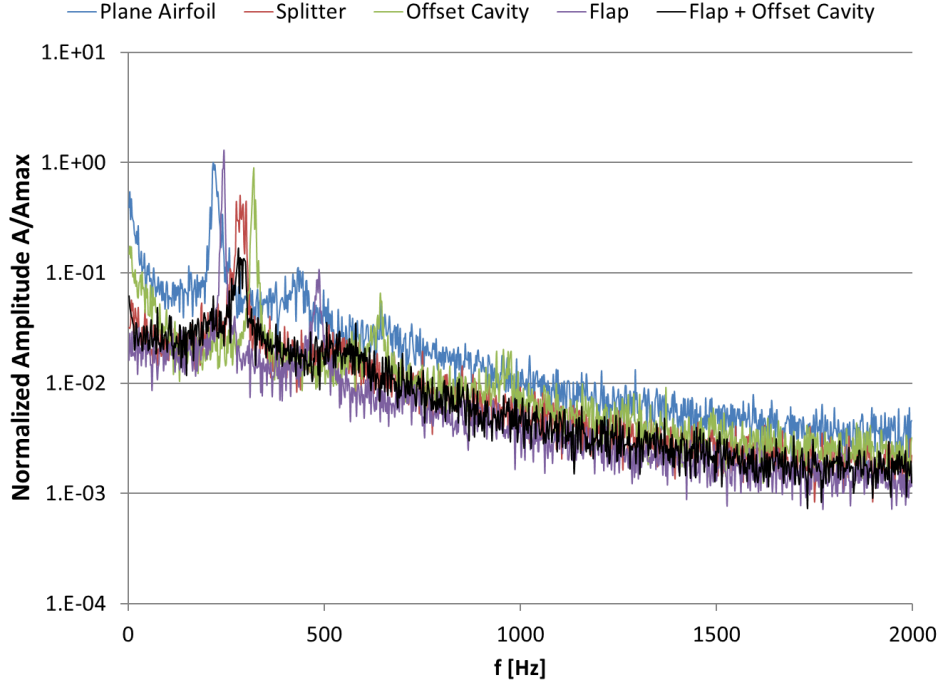


**Figure 22: Frequency spectrum from the hot wire measurements for the examined TE devices and the plane airfoil.**

For flatback airfoils the Strouhal number can be defined as:

$$St = \frac{fh}{U_\infty} \quad (1)$$

For the plane airfoil  $St = 0.24$  and  $St = 0.31$  when the splitter is used, which is really close to the experimental measurements in [15] ( $St = 0.24$  for the plane airfoil and  $St = 0.30$  for the splitter). All other devices also increased  $St$ , with the highest increase measured for the Offset Cavity ( $St = 0.35$ ).

It is interesting to note the similarity of the plane airfoil with the Offset Cavity case. The peak amplitude of the main frequency is similar in the two cases and the second and third peaks also appear. This evidence combined with the observations in the previous section (V.C: Stereo PIV results) suggest that the flow downstream of the Offset Cavity is similar to the flow downstream of the plane airfoil TE, only it scales with the cavity height rather than the airfoil TE height. The drag reduction is achieved because the vortex shedding occurs further away from the wing TE and the base pressure is increased. At the same time the shedding occurs at a higher frequency with smaller variations and this requires less energy.

## VI. Conclusions

A flatback airfoil was tested experimentally with various TE drag reduction devices. The blunt TE airfoil was based on a thin TE airfoil optimized for use on a LIR. The thin TE airfoil had a design  $Cl$  of 0.8 so the question was how the TE devices would affect the airfoil performance around the design  $Cl$  region.

Along with previously tested devices, such as cavities and splitter plates, a new device (Flap) was tested on its own and in combination with the other devices. The Flap is different to thin airfoil slotted flaps in the sense that the flow coming from the airfoil top side feeds its pressure side, rather than the high speed flow coming from the airfoil pressure side feeding its suction side. To the best of the authors' knowledge this is the first investigation of such a device on a flatback airfoil.

Lift and drag were extracted from pressure measurements at  $Re_c = 1.5e6$ . All devices improved the  $L/D$  of the plane airfoil. The best performing device was one of the new devices (Flap + Offset Cavity), which increased  $L/D$  by 131% (from 19.1 to 44.0) at the design  $Cl = 0.8$ . The Extended Cavity device increased  $Cl_{max}$  by 17% (from 1.69 to 1.98) with a modest improvement (+12%) in  $L/D$  at design  $Cl$ . The drag reduction appears to scale linearly with the increase in base pressure caused by the devices. The flatback airfoil experienced 3D separation of the SC type with or without the TE devices.

Stereo PIV and hot wire measurements were performed on the best performing devices (Offset Cavity, Splitter, Flap, Flap + Offset Cavity) to examine the flow characteristics at the wake of the wing. Regarding the mean flow, all devices move the saddle point in the wake downstream compared to the plane airfoil case. The  $Re$  stress contours suggest that all devices reduced the unsteadiness downstream of the wing TE and that the device that restricted the flow variations the most is the Flap + Offset Cavity.

Hot wire measurements show that all devices increase the main shedding frequency of the vortices downstream of the TE. Multiples of the main frequency are observed both for the plane airfoil and for the drag reduction devices. The Flap + Offset Cavity achieved the highest reduction in the main frequency amplitude peak by 84%. The implications of this frequency shift and amplitude reduction regarding noise generation and fatigue loads require further investigation.

The flow downstream of the Offset Cavity is very similar to that downstream of the plane airfoil TE, but it scales with the cavity height rather than the TE height. As previously observed for a normal cavity, the mechanism here is to move vortex roll up downstream away from the wing TE. It is noted that the position of the splitter plates for the cavity was not optimized and perhaps greater gains could be obtained.

The overall conclusion is that all devices transform the large, slow variations of the flow downstream of the wing TE, into quicker fluctuations of lower amplitude. The most effective device in terms of L/D increase is also the one that limited the flow variations the most, suggesting that large and slow variations are more “expensive” compared to the small and fast ones.

It is worth noting that this is a proof-of-concept investigation for the Flap and that the device was not optimized in any way. The effect of parameters such as Flap angle of attack, chord length, profile and position remain to be examined. Further research could also investigate the ability of the new Flap device to actively control loads on a wing.

## VII. Acknowledgements

This work is part of the INNWIND.EU project supported by European Union under the Seventh Framework Programme (FP7).

## VIII. References

- [1] Baker, J., Mayda, E., and Van Dam, C. "Experimental analysis of thick blunt trailing-edge wind turbine airfoils," *Journal of Solar Energy Engineering* Vol. 128, No. 4, 2006, pp. 422-431.
- [2] Baker, J. P., Van Dam, C., and Gilbert, B. L. "Flatback airfoil wind tunnel experiment," *Sandia Report, SAND2008-2008*. Sandia National Laboratories, Albuquerque, NM, USA, 2008.
- [3] Hoerner, S. F. "Base drag and thick trailing edges," *Journal of the Aeronautical Sciences (Institute of the Aeronautical Sciences)* Vol. 17, No. 10, 1950, pp. 622–628.
- [4] Baker, J., and van Dam, C. "Drag reduction of blunt trailing-edge airfoils," *International Colloquium on: Bluff Bodies Aerodynamics & Applications*. Italy, July, 2008.
- [5] Tanner, M. "A method for reducing the base drag of wings with blunt trailing edge," *Aeronautic Q.* Vol. 23, 1970, pp. 15-23.
- [6] Choi, H., Jeon, W.-P., and Kim, J. "Control of flow over a bluff body," *Annu. Rev. Fluid Mech.* Vol. 40, 2008, pp. 113-139.
- [7] Viswanath, P. "Flow management techniques for base and afterbody drag reduction," *Progress in Aerospace Sciences* Vol. 32, No. 2, 1996, pp. 79-129.
- [8] Molezzi, M. J., and Dutton, J. C. "Study of subsonic base cavity flowfield structure using particle image velocimetry," *AIAA Journal* Vol. 33, No. 2, 1995, pp. 201-209.
- [9] Petrusma, M. "Base pressure recovery for segmented trailing edge aerofoils," *Australasian Fluid Mechanics Conference, 11 th, Univ. of Tasmania, Hobart, Australia*. 1992, pp. 787-790.
- [10] Bearman, P. "Investigation of the flow behind a two-dimensional model with a blunt trailing edge and fitted with splitter plates," *Journal of Fluid Mechanics* Vol. 21, No. 02, 1965, pp. 241-255.
- [11] Williamson, C. H. "Vortex dynamics in the cylinder wake," *Annual Review of Fluid Mechanics* Vol. 28, No. 1, 1996, pp. 477-539.
- [12] Roshko, A. "On the wake and drag of bluff bodies," *Journal of the Aeronautical Sciences* Vol. 22, No. 2, 1955, pp. 124-132.

- [13] Krentel, D., and Nitsche, W. "Investigation of the near and far wake of a bluff airfoil model with trailing edge modifications using time-resolved particle image velocimetry," *Experiments in Fluids* Vol. 54, No. 7, 2013, pp. 1-16.
- [14] Thompson, B., and Lotz, R. "Flow around a blunt and divergent trailing edge," *Experiments in Fluids* Vol. 33, No. 3, 2002, pp. 374-383.
- [15] Barone, M. F., and Berg, D. "Aerodynamic and aeroacoustic properties of a flatback airfoil: an update," *AIAA Paper*, No. 271, 2009.
- [16] Kim, T., Jeon, M., Lee, S., and Shin, H. "Numerical simulation of flatback airfoil aerodynamic noise," *Renewable Energy* Vol. 65, No. 0, 2014, pp. 192-201. doi: <http://dx.doi.org/10.1016/j.renene.2013.08.036>
- [17] Mertes, C., Singh, M., Strike, J., Hind, M., Babbitt, A., Baker, J., Naughton, J., and Sitaraman, J. "A Study of Flatback Airfoils in Dynamic Motion " *AIAA Paper*, No. ro349, 2011.
- [18] Roshko, A. "On the drag and shedding frequency of two-dimensional bluff bodies," *NASA TN 3169*. 1954.
- [19] Mayda, E. A., van Dam, C., Chao, D. D., and Berg, D. E. "Flatback airfoil wind tunnel experiment." Sandia National Laboratories, 2008.
- [20] Kahn, D. L., van Dam, C., and Berg, D. E. "Trailing edge modifications for flatback airfoils." Sandia National Laboratories, 2008.
- [21] Nash, J. F. "A discussion of two-dimensional turbulent base flows," *Reports and Memoranda No. 3468*. ARC, 1965.
- [22] Tanner, M. "Reduction of base drag," *Progress in Aerospace Sciences* Vol. 16, No. 4, 1975, pp. 369-384.
- [23] Berg, D. E., and Zayas, J. R. "Aerodynamic and aeroacoustic properties of flatback airfoils," *AIAA Paper*, No. 1455, 2008.
- [24] Chaviaropoulos, T., Sieros, G., Irisarri, A., Martinez, A., Munduate, X., Grasso, F., Ceyhan, O., Madsen, H. A., Rasmussen, L. B. F., and Zahle, F. "New aerodynamics rotor concepts specifically for very large offshore wind turbines," *INNWIND.EU D2.11 Deliverable*. 2015.
- [25] Barlow, J. B., Rae, W. H., and Pope, A. *Low-speed wind tunnel testing*. New York: John Wiley & Sons, 1999.
- [26] van Dam, C., Mayda, E. A., Chao, D. D., and Berg, D. E. "Computational Design and Analysis of Flatback Airfoil Wind Tunnel Experiment," *Sandia Report SAND2008-1782*. Albuquerque, NM, USA, 2008.
- [27] Westerweel, J. "Theoretical analysis of the measurement precision in particle image velocimetry," *Experiments in Fluids* Vol. 29, No. 1, 2000, pp. S003-S012.
- [28] Foucaut, J. M., Miliat, B., Perenne, N., and Stanislas, M. "Characterization of different PIV algorithms using the EUROPIV synthetic image generator and real images from a turbulent boundary layer," *Particle Image Velocimetry: Recent Improvements*. Springer, 2004, pp. 163-185.
- [29] Manolesos, M., and Voutsinas, S. G. "Study of a stall cell using stereo particle image velocimetry," *Physics of Fluids* Vol. 26, No. 4, 2014, p. 045101. doi: <http://dx.doi.org/10.1063/1.4869726>
- [30] Manolesos, M., Papadakis, G., and Voutsinas, S. G. "Experimental and computational analysis of stall cells on rectangular wings," *Wind Energy* Vol. 17, No. 6, 2013. doi: 10.1002/we.1609
- [31] Broeren, A. P., and Bragg, M. B. "Low-frequency flowfield unsteadiness during airfoil stall and the influence of stall type," *AIAA Paper*, No. 2517, 1998.